RSC Mechanochemistry

ROYAL SOCIETY OF CHEMISTRY

PAPER

View Article Online
View Journal | View Issue

Cite this: *RSC Mechanochem.*, 2025, **2**, 732

Mechanochemistry of phosphate esters with external electric fields†

Zhaoran Zhu * and James P. Ewen *

The growth of tribofilms from the mechanochemical decomposition of lubricant additives is crucial to prevent wear of sliding metal surfaces. For some applications, such as electric vehicles and wind turbines, lubricants can be exposed to electric fields, which may affect tribofilm growth. Experimental tribometer results have shown conflicting results regarding antiwear tribofilm growth and wear under external electric potentials. Moreover, the effect of electric fields on the mechanochemical decomposition of lubricant additives remains unclear. Here, we use nonequilibrium molecular dynamics (NEMD) simulations to study the mechanochemical growth of a polyphosphate tribofilm from trialkyl phosphate molecules under external electrostatic fields. The decomposition rate of phosphate esters increases exponentially with the applied stress and temperature. The electric field generally accelerates the molecular decomposition, both by enhancing the interfacial stress and reducing the steric hindrance for nucleophilic substitution. The Bell model is used to analyse the electro-, mechano- and temperature-dependent decomposition process. Under weak electric fields, the activation energy for molecular decomposition increases due to the competition between electric field- and shear-induced deformations. For stronger fields, the activation energy decreases linearly with increased electric field strength and this dominates over the shear-induced molecular rotation. The resultant non-monotonic variation in the activation energy for molecular decomposition with electric field strength explains the conflicting effects of electric potential on tribofilm growth observed experimentally. The activation volume decreases linearly with increasing electric field strength, indicating a reduced dependence of the decomposition on shear stress as the electric field dominates. Asymmetric tribofilm growth is observed between surfaces with external electric fields, which is consistent with the experimental observations. This study presents atomistic insights for the coupling of electro- and mechano-catalysis of an industrially-important molecular decomposition process.

Received 7th May 2025
Accepted 2nd July 2025

DOI: 10.1039/d5mr00064e

rsc.li/RSCMechanochem

Introduction

Mechanochemistry involves accelerating chemical reactions with mechanical force.[1] It is playing an increasingly important role in organic and materials synthesis as well as polymer modifications and recycling.[1] An emerging area in mechanochemical synthesis is combining mechanical forces with other energy sources, such as electric fields.[2] Several studies have suggested that the cooperation of the electric field with mechanical force can reduce the activation barrier of chemical reactions.[3–6] Another prominent example is contact-electrocatalysis, which utilizes electron transfer occurring at chemically inert solid–liquid interfaces to stimulate redox reactions.[7]

Probably the most economically valuable application where mechanochemistry plays a central role is anti-wear lubricant additives,[8] such as zinc dialkyldithiophosphate (ZDDP).[9] The growth of protective tribofilms from ZDDP is accelerated by shear stress.[10] This means that ZDDP tribofilms can be formed without high temperatures, ensuring wear protection even in cold environments.[11] For some applications, such as electric vehicles[12] and wind turbines,[13] lubricant additives can also be exposed to electric fields. For dielectric materials, intense electric fields can be generated just outside of the sliding contact due to the tribocharging.[14] Previous studies have shown contradictory results regarding the effect of external electric fields on tribofilm growth and wear.[15,16] ZDDP films have been successfully be grown on metal surfaces from a base oil at relatively low temperatures and without rubbing by the application of large voltages across the contact.[17] Voltage across a tricresyl phosphate (TCP)-lubricated contact promoted tribofilm formation,[18] and using dilauryl hydrogen phosphate greatly reduced friction.[19] It was found that sliding under applied electric potentials, zinc organodithiophosphate (ZDP) was more effective in forming a friction-

Department of Mechanical Engineering, Imperial College London, London SW7 2AZ, UK. E-mail: zhaoran.zhu22@imperial.ac.uk; j.ewen@imperial.ac.uk

† Electronic supplementary information (ESI) available: Additional figures and results for coefficients from the extended Amontons–Coulomb friction equation, angular velocity, the change in the number of bonds, polyphosphate tribofilm, and reaction parameters and fits using the Bell model. See DOI: https://doi.org/10.1039/d5mr00064e

and wear-reducing tribofilm, compared to the uncharged condition.[20] ZDDP also showed a friction and wear reduction under a positive oxidising potential, which was attributed to increased disulfide formation.[21] For sulphur-based additives, increased wear has been noted at the anodic surface compared to the cathodic surface, which was due to rapid corrosion.[22] For phosphorus-based additives, however, wear was suppressed on both anodic and cathodic surfaces.[22] Thicker ZDDP tribofilms have been noted when electric fields were applied across the sliding contact.[23] It was shown recently that the tribofilm growth from ZDDP-containing base oils was suppressed by relatively low electric potentials and more severe wear was observed at the anodic surface.[24] However, other recent studies using ZDDP reported that the electric potential formed a tribofilm much thicker than at open circuit potential.[25,26] It is not clear what effects applied electric potentials have on the molecular-scale processes leading to tribofilm growth. Therefore, a detailed understanding of the nanoscale mechanochemical behaviours of lubricants additives in the presence of external electric field is urgently required. This will help to explain the macroscale tribological phenomena at electrified contacts, such as bearing failure under electric current,[16] reduced corrosive wear,[15] and electric field-altered tribofilm formation. Meanwhile, this helps us to understand the effectiveness of current lubricant additives and expedite the discovery of new molecules for modern machinery operated under electric fields.

Nonequilibrium molecular dynamics (NEMD) simulations have been widely employed to investigate the effect of both shear stress[27,28] and electric fields[29] on chemical reactivity. However, only a handful of studies have combined NEMD simulations with both shear and electric fields applied. Probably the most studied system with NEMD simulations using combined shear and electric fields is the electrotunable friction of ionic liquid (IL) lubricants,[30–32] as recently reviewed.[33] Of particular interest for this study, NEMD simulations with ReaxFF have recently been used to investigate the tribochemical reactions between a phosphonium phosphate IL and iron surfaces under the combined effects of applied shear and electric fields.[34] Other studies have also looked at the effect of electric fields on the friction of other systems in sliding NEMD simulations, including poly-α-olefin base oils[35] and zwitterionic molecules.[36]

In this study, we use NEMD simulations with ReaxFF[37] to investigate the effect of electric fields on the mechanochemical decomposition of phosphate ester-based anti-wear additives. We also study the influence of the electric field on tribofilm growth and its chemical composition. This study provides atomistic insights into electro-mechano-chemical reactions and improves our understanding of tribological behaviours inside electrified contacts. We anticipate that the methodology showcased here can be used to virtually screen lubricant additives for applications where they are exposed to external electric fields, such as electric vehicles and wind turbines.

Methods

A primary alkyl phosphate, tri-*n*-butyl phosphate (TNBP), was selected for this study, as shown in Fig. 1a. Alkyl phosphates such as TNBP are used as additives in gear lubricants, industrial lubricants, and transmission fluids.[38,39] They have also been employed in their pure form as high-temperature vapour phase lubricants.[40] TNBP exhibits intermediate thermal stability and reactivity between secondary alkyl and aryl phosphate esters.[41] We have previously investigated the decomposition of TNBP under shear[42] and in the presence of electric fields.[43] Here, we study the decomposition of TNBP molecules under the combined effects of temperature, shear, and electric fields. We use confining magnetite surfaces, mimicking the asperity–asperity contacts occurring in tribology experiments.[44]

The confined system was constructed using the Materials and Process Simulations (MAPS) platform developed by Scienomics SARL. The α-$Fe_3O_4(001)$ surfaces had dimensions of 5.0 nm in the *x*- and *y*-directions, and a thickness of 1.1 nm in the *z*-direction. Periodic boundary conditions were used in the *x*- and *y*-directions, and a fixed boundary was used in the *z*-direction. Initially, the two surfaces were separated by 3.0 nm of vacuum in the *z*-direction. 48 TNBP molecules were randomly inserted between two iron oxide surfaces, resulting in a surface coverage of 1 molecule per nm^2. This is representative of the monolayer adsorption of phosphate esters on ferrous surface, as observed in experiments both from the vapour phase[45] and from base oil solution.[46]

Simulation details

All of the NEMD simulations were performed in the large atomic/molecular massively parallel simulator (LAMMPS) software.[47] Velocity Verlet[48] integration was employed with a timestep of 0.25 fs. We use the version of ReaxFF[37,49] implemented in LAMMPS,[50,51] with the parameters from Khajeh *et al.* for C/H/O/Fe/P systems.[52] Dissociation and tribofilm growth of phosphate esters has been extensively studied using these ReaxFF parameters.[41–43,53–55] The parameters have been validated for single-molecule dissociation of TNBP against density functional theory.[41]

The system was first energy minimized using the conjugate gradient method. Then, the top surface was moved down at a speed of 10 m s^{-1} until reaching a liquid density of TNBP in agreement with the experimental value (0.97 g cm^{-3}).[56] The lowermost layer of atoms in the bottom surface was fixed. The target pressure (P_z = 1–3 GPa) was then applied to the upper surface to compress the TNBP molecules, by adding a constant normal force to the topmost layer of atoms in the upper surface. The system was then equilibrated at 300 K for 0.1 ns under the target normal pressure. A Langevin thermostat[57] with a damping coefficient of 25 fs was applied to the middle layer of atoms in the surfaces to control the temperature. A representative snapshot of the system after energy minimization and equilibration is presented in Fig. 1b. After equilibration, the temperature was increased (T = 550–750 K) and an electrostatic field (ε_z = 0.10–1.00 V $Å^{-1}$) and sliding velocity (v_x = 10 m s^{-1}) were applied simultaneously. During the NEMD simulations, the pressure was maintained by fixing the *z*-direction separation distance between the bottom and top wall at the end of the equilibration process. The sliding velocity was imposed by

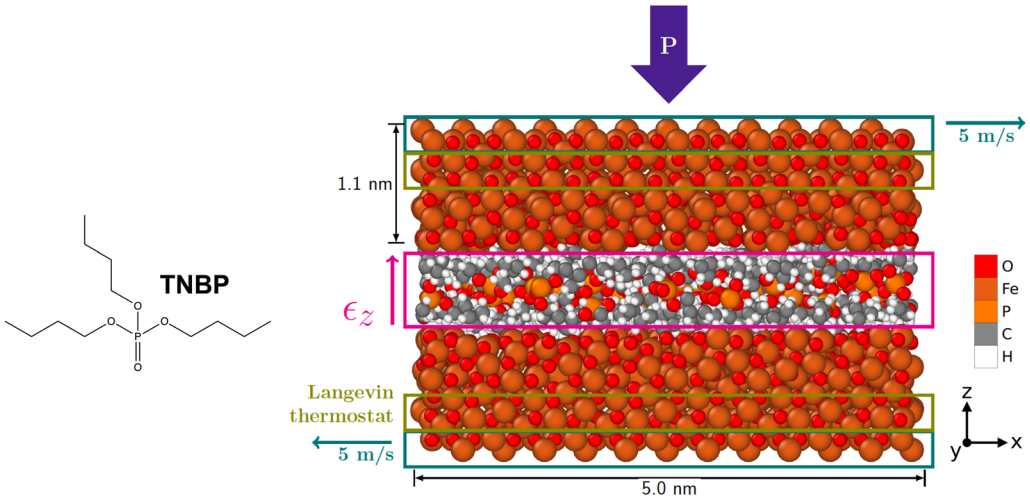

Fig. 1 Molecular structure of the tributyl phosphate (TNBP) and the simulation system setup rendered with OVITO.[58]

applying equal and opposite velocities (± 5 m s^{-1}) along the x-direction to the outer layer of atoms in the two surfaces. These production simulations under an electric field were performed for 1.0 ns.

Modelling electric field interactions

As demonstrated in our previous study,[43] under electric fields, the QTPIE method[59] predicts more accurate charge distribution profile and electric field induced polarization than the standard QEq[60] charge equilibration method. Herein, we use the same QTPIE implementation[61] for all the ReaxFF NEMD simulations, which is now implemented in LAMMPS.[47]

The QTPIE model adopts the idea of overlapping charge distributions between neighbouring atoms, which effectively shields the long-range charge transfer.[59,61–63] The atomic charges are updated by minimizing the electrostatic energy, where the effective electronegativity is used instead of the atomic electronegativity.[59] Detailed mathematical derivations can be found in our previous paper[43] and other related studies.[61,64] With the presence of an electric field, the effective electronegativity for the ith atom is:

$$\chi_{\mathrm{eff},i} = \frac{\sum_j \left(\chi_i^0 - \chi_j^0 + \vec{r_j}\cdot\vec{\varepsilon}\right) S_{ij}}{\sum_{j'} S_{ij'}} - \vec{r_i}\cdot\vec{\varepsilon} \quad (1)$$

where χ_i^0 and χ_j^0 are the atomic electronegativities for i^{th} and j^{th} atom, $\vec{\varepsilon}$ is the electric field in units of V Å^{-1}, and S_{ij} is the overlap integral of the atomic orbitals of i^{th} and j^{th} atoms.[59] Similar to our previous study,[43] here we used the primitive Gaussian-Type Orbitals (GTO) to calculate the overlap integral S_{ij}, with the exponential constants from Chen and Martínez.[65] Since they have demonstrated the negligible absolute error when using GTO compared to the more accurate Slater-Type Orbitals (STO).[66] More details about the validation and implementation of the QTPIE method can be found elsewhere.[59,61,63]

In this study, a uniform electrostatic field was applied along the positive z-direction ($\varepsilon_z = 0.10$–1.00 V Å^{-1}), as shown in Fig. 1. This approach mimics tribology experiments in which an electric field is applied across a lubricated contact.[67,68] The requirement for large electric field strengths is a common limitation of NEMD simulations.[29] The strength of the electric fields used in our NEMD simulations is somewhat higher than those typically applied in nanoscale tribology experiments using atomic force microscopy ($\sim$0.1 V Å^{-1})[69] and macroscale tribometer experiments under elastohydrodynamic lubrication conditions ($\sim$0.02 V Å^{-1}).[70] However, for tribology experiments under boundary lubrication conditions, where the lubricant film thickness is normally on the angstrom scale,[71] electric field strengths approaching those used in our NEMD simulations can be realistically expected. The surface electric potential corresponding to the maximum electric field used here is approximately 10.0 V, which has been widely adopted in electro-mechano-chemical reactions, both in experiments[69,72] and ReaxFF NEMD simulations.[35,43,73,74]

Reaction kinetics analysis

When subjected to external stress, phosphate esters and ZDDPs decompose and form a polyphosphate tribofilm at moderately elevated temperatures.[9,10,42,75–77] The molecular decomposition and subsequent tribofilm growth has been widely modelled as stress-augmented thermally activated (SATA) processes.[78] In a SATA process, the applied stress serves as the mechano-chemical driving force for bond cleavage and affects the reaction rate constant, k, as described by the Bell model:[79]

$$k = A \exp\left(-\frac{E_a - \tau \Delta V^*}{k_B T}\right) \quad (2)$$

where k is the rate constant for the reaction, A is the pre-exponential factor (or frequency factor), E_a is the activation energy, τ is the shear stress, ΔV^* is the stress activation volume, k_B is the Boltzmann constant, and T is the temperature. For tribofilm growth from anti-wear additives, it has been

demonstrated that the shear stress, rather than the normal stress, drives the mechanochemical reaction.[10,42,75–77] Our previous MD simulations of high-temperature TNBP decomposition without applied shear stress showed that external electric fields decreased E_a on iron oxide surfaces.[43] It is not clear how the external electric field will affect the mechanochemical reaction and parameters in the Bell equation. The formalism employed to study mechanochemistry can also be applied to explore how external electric fields can catalyse and control reactions.[80,81] Some studies have used Bell-like models to describe the combined effects of electric fields and stress on electro-mechano-chemical (or tribo-electro-chemical) reactions.[72,82]

The rate-limiting step of polyphosphate tribofilm growth is the initial removal of alkyl or aryl substituents, which has been confirmed through NEMD simulations for phosphate esters[42] and experiments for ZDDP.[76,77] In this study, the reaction rate constant was determined from the decay of the number of intact TNBP molecules over the course of the simulation. Molecules with any of their C–O, P–O, or C–C bonds broken were considered as non-intact. In the majority of cases, the C–O bond was the first bond to break, followed by the P–O bond, which is consistent with previous NEMD simulations of TNBP.[42] Atomic trajectories and bonding information, using a bond order cutoff of 0.3, were recorded every 1.0 ps.

Results and discussion

The shear stress, rather than the normal stress, has been shown as the dominant driving force for the mechanochemical tribofilm growth from antiwear lubricant additives lubricants.[10,75–77] Firstly, we compare the change in shear stress with normal stress under different external electric fields, as shown in Fig. 2. The steady-state shear stress and normal pressure were averaged over both walls and time-averaging was performed over the final 0.8 ns of the production run. At all the studied temperatures, the shear stress increases linearly with the applied pressure with a finite intercept, as described by the extended Amontons–Coulomb friction equation:[83]

$$\tau = \mu\sigma + \tau_0 \quad (3)$$

where τ is the shear stress, μ is the friction coefficient, σ is the normal stress, and τ_0 is the Derjaguin offset. The Derjaguin offset τ_0 can be related to the surface adhesion.[84] The dotted line in Fig. 2 is fitted to eqn (3) and μ and τ_0 are extracted from the slope and the intercept of the curve, respectively. The values of μ and τ_0 are summarized in Table S1.† At all applied normal stresses, the shear stress decreases with increasing temperature, which leads to a negligible change in μ, but a decrease in τ_0.

It is noteworthy that, when the electric field is applied, the normal stress distribution between the two surfaces becomes asymmetric, as observed in previous MD simulations.[34] At the maximum applied electric field strength, 1 V Å^{-1}, the normal stress acting on the top wall increases by approximately 0.5 GPa compared to the applied value, while the normal stress on the bottom wall decreases by 0.5 GPa. Thus, although the external electric field changes the normal stress distribution between the two surfaces, the average normal stress remains the same as when no electric field is applied. Stiffening of the adsorbed molecular layer has also been observed in hydrogen bond networks formed by water under electric fields.[85]

The extended Amontons–Coulomb friction model holds with the application of external electric fields. The shear stress increases with increasing external electric field strength. A clearer comparison between the shear stress under electric fields and without the electric field is presented in the ESI (Fig. S1).† The increment in shear stress due to the electric field is more pronounced for lower normal stress. This is likely because, when the normal stress is lower, the separation gap between two sliding surfaces is larger, and the enhancement of surface–lubricant interactions under the electric field is more pronounced. This enhancement is less apparent when subjected to higher loads, where the interactions were already more frequent due to the smaller gap between two surfaces.

Snapshots of the TNBP molecules being sheared at 700 K and 2 GPa with electric fields are presented in Fig. 3. The through-thickness number density profile for the various atoms in the system was computed and averaged over the course of the simulation. For the case without the electric field, the TNBP molecules were equally reacting with both surfaces, as indicated by the symmetric distribution around the middle of the gap. Compared to our previous study under thermally activated decomposition,[43] the peak density for all the atoms of TNBP molecules were increased in this study. This is due to the compression from the applied normal stress, leading to a narrower separation gap. When exposed to an electric field, rearrangement of the TNBP molecules was observed, which is due to the alignment of molecular dipoles with the electric field direction.[43] As a result, the polar head group including the P and O atoms, were pushed towards the bottom surface with higher electric potential. Conversely, the nonpolar hydrocarbon clusters were mainly located near the top surface with lower electric potential. This is consistent with the experimental observations that the formation of polyphosphate tribofilm from ZDDP is enhanced on the positively charged surface.[25] The spatial rearrangement of the TNBP molecules was more pronounced as the electric field strength was increased. Similar behaviours were also observed at other pressures, as shown in Fig. S3.†

When an electric field is applied, the TNBP molecules experience a torque that aligns the molecular dipole with the field.[43] When the sliding velocity is applied along the x-direction, an additional torque about the y-axis is generated. The angular velocities along y-axis during sliding are shown in the ESI (Fig. S2).† As the normal (and shear) stress is increased, the magnitude of the angular velocity ω_y is increased, indicating enhanced rotational motions.[43] Similarly, ω_y increased in the presence of an electric field and exhibited a broader distribution.

Fig. 3 shows the significant overlap of TNBP carbon and surface iron atoms, which catalyses the C–O bond dissociation in the TNBP molecules.[40,41] On the other hand, P–O cleavage in TNBP by nucleophilic substitution is accelerated by the overlap

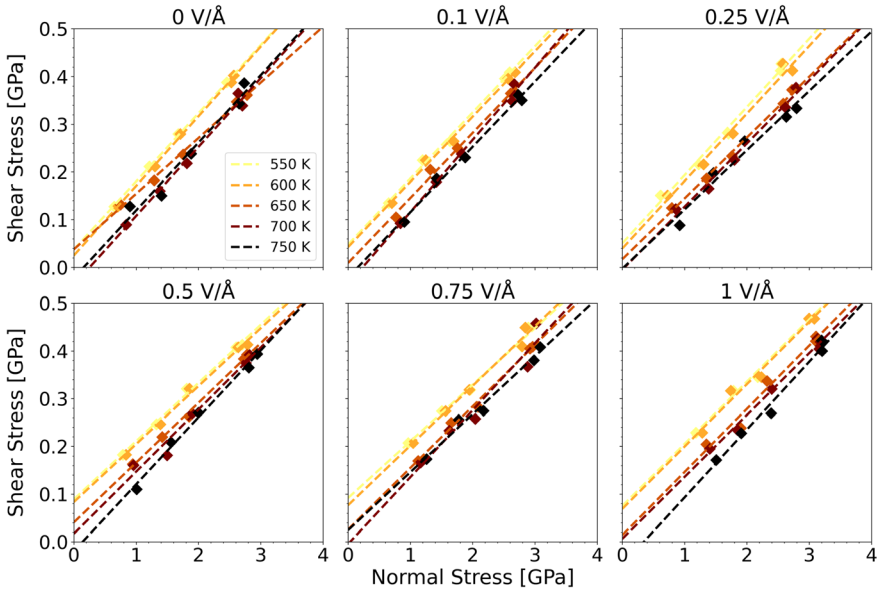

Fig. 2 Variation in shear stress with normal stress under different temperatures and applied electric fields.

of phosphorus atoms in molecules and oxygen atoms in the iron oxide surfaces.[41] Mechanochemical decomposition leads to the formation of alkyl cations and phosphate anions, which deposit onto the surfaces. As shown in Fig. 4, even without the electric field, carbon and phosphorus atoms in TNBP molecules form covalent bonds with the surfaces. As the electric field strength increases, the number of carbon-surface, oxygen-surface and phosphorus-surface bonds increases, indicating that there is more TNBP decomposition on the catalytic surfaces.[43] Enhanced surface bond formation under electric fields was also observed in the system sheared at 700 K and 1 GPa, as shown in the ESI (Fig. S4).† Compared to Fig. 4 and S4† shows that higher

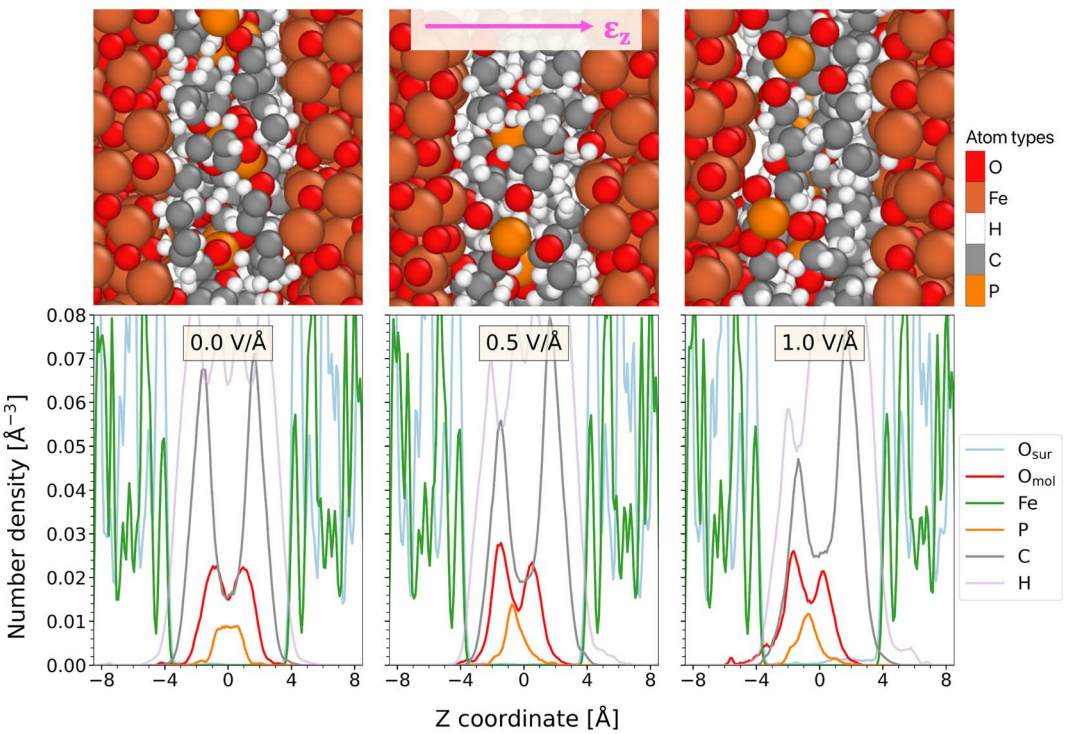

Fig. 3 Simulation snapshots of TNBP molecules confined between two Fe_3O_4 surfaces at 700 K and 2 GPa, under different electric field strengths (top), corresponding through-thickness number density profiles for different atom types (bottom). For both figures, the electric field was applied along the positive z direction as shown by the pink arrow.

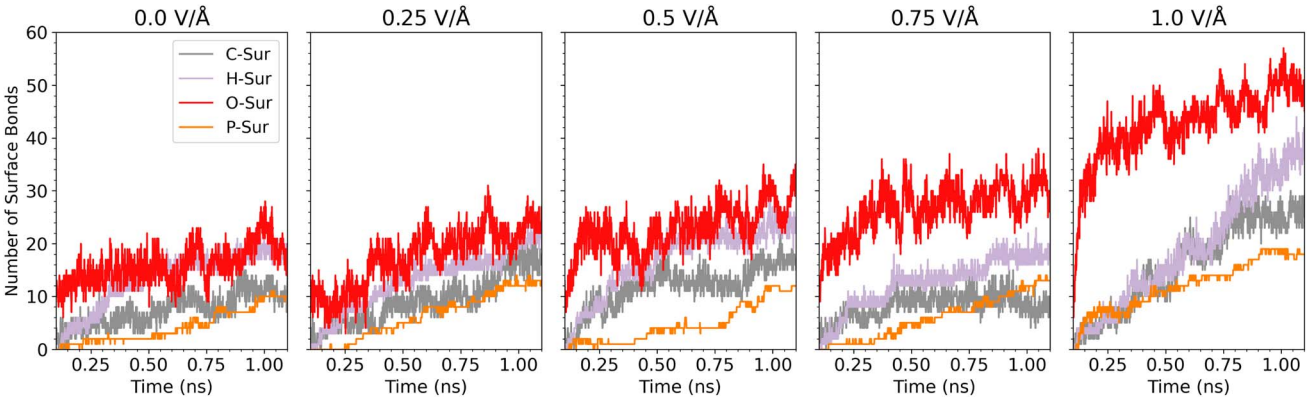

Fig. 4 Number of covalent bonds formed between TNBP molecules and the Fe_3O_4 surfaces under different electric fields under 2 GPa at 700 K.

interfacial stress promotes tribofilm formation on both unelectrified and electrified surfaces.

Phosphate esters decompose and form polyphosphate tribofilms on the ferrous surfaces, which is responsible for their anti-wear performance.[54] Nucleophilic substitution is a key reaction pathway for the growth of polyphosphate,[41,53] through replacing the P–O–R bonds by the P–O–P bonds in the phosphate esters. Here, we also compared the polymerization after TNBP decomposition, as shown in Fig. 5. Sliding at 700 K and 2 GPa, in the reference case without an electric field ($\varepsilon_z = 0$ V Å^{-1}), phosphates primarily formed dimers, with a few forming trimers, and the largest observed cluster was a tetramer. This is similar to previous NEMD simulations with TCP on iron surfaces.[54] The chain length of polyphosphate observed in our simulations is consistent with the averaged chain length of 2.5 monomers found in tribological experiments using XPS measurements.[86,87] This is also consistent with the cross-second MD simulations.[88] At lower normal stress, only monomers, dimers, and a few trimers formed, as shown in the ESI (Fig. S5).† This suggests that higher stress enhances polyphosphate growth and increases the degree of polymerization. With an electric field, the transformation from monomers to polyphosphates was accelerated. Moreover, longer polyphosphates including pentamers and above were observed for $\varepsilon_z = 0.5$ V Å^{-1}, and particularly 1 V Å^{-1} (Fig. 5). When exposed to an electric field, phosphates undergo conformational changes that rotate

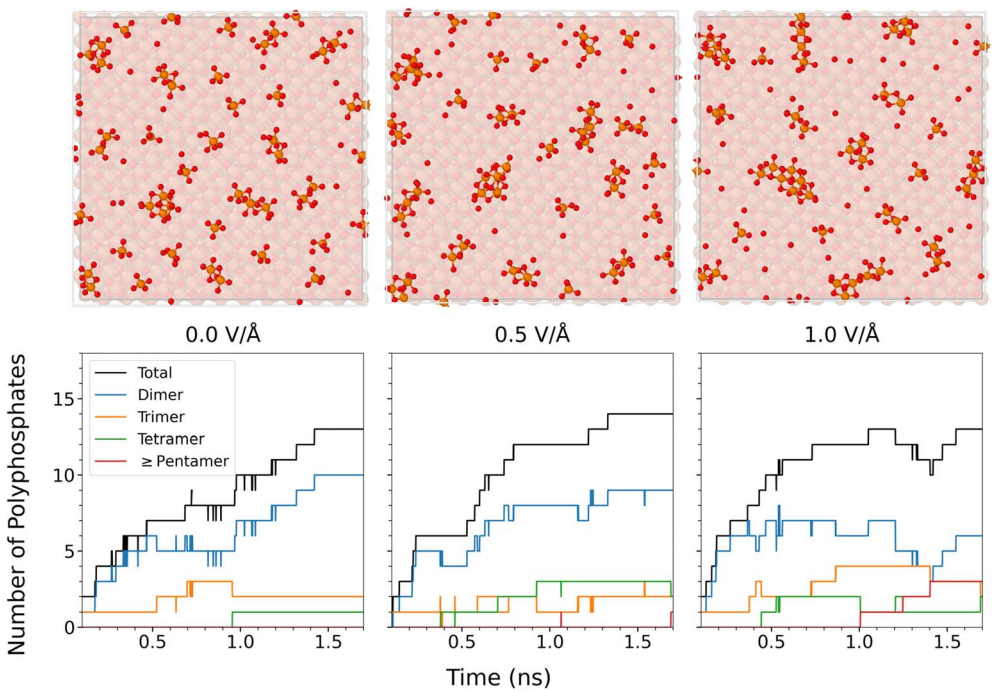

Fig. 5 Change in the number of polyphosphates with time at 700 K and 2 GPa, under different electric field strengths. Snapshots of the polyphosphates were taken at the end of the calculation time (1.7 ns). P atoms were coloured in orange and O atoms in red. C and H atoms were omitted for clearer illustration.

the polar head and the nonpolar alkyl groups (Fig. 3). Since the alkyl cations are pulled towards the opposite surfaces, the electric field-induced dipole alignment may reduce the steric hindrance of the polar head (PO_4^{3-}) between neighbouring TNBP molecules. Subsequently, nucleophilic substitution and polymerization are favoured under the applied electric field. Previous study has reported that long-chained polyphosphate typically undergoes depolymerization during continuous rubbing, due to the lack of stabilizing cations.[89] The remaining highly-polymerized phosphates under electric fields observed here, might be ascribed to the electrostatic stabilization of the charged transition state and products of the dissociation reaction, as reported in our previous study.[43]

The electro-mechano-chemical dissociation rate of TNBP molecules under electric fields was investigated over a range of electric field strengths, temperatures and stresses. Fig. 6a and b show the decay in the number of intact phosphate molecules with sliding time, at a fixed temperature (700 K) and fixed pressure (2 GPa), respectively. The decay in the number of intact molecules with time is fitted with an exponential function, indicating a first-order reaction.[42] A rate constant is extracted from the exponential decay fits for each condition. Without the electric field, the rate of TNBP decomposition increased with increasing temperature and shear stress. These observations are consistent with previous SATA experiments[10,75] and NEMD simulations.[42,54] The rate of TNBP decomposition generally increases with electric field strength, which is consistent with our previous MD simulations without compression or sliding.[43] At the highest normal stress (3 GPa) studied here, the enhancement of the rate constant due to electric fields is less apparent than at lower stress. This is because under high normal stress, the decomposition reaction is primarily determined by shear stress. Similarly, at the highest temperature (750 K), the effect of the electric field on TNBP decomposition is less prominent.

Mechanochemical parameters

Fig. 7 shows the combined dependence of mechanochemical reaction rates, from the electric field, temperature and shear stress. The rate constants were taken from Fig. 6 and the shear stress values were from Fig. 2. All of the data at each electric field strength was described using 3D fits to the Bell model[79] (eqn (2)).[42,54] As the electric field strength increases, an increase in the rate constants for TNBP decomposition was observed in Fig. 7.

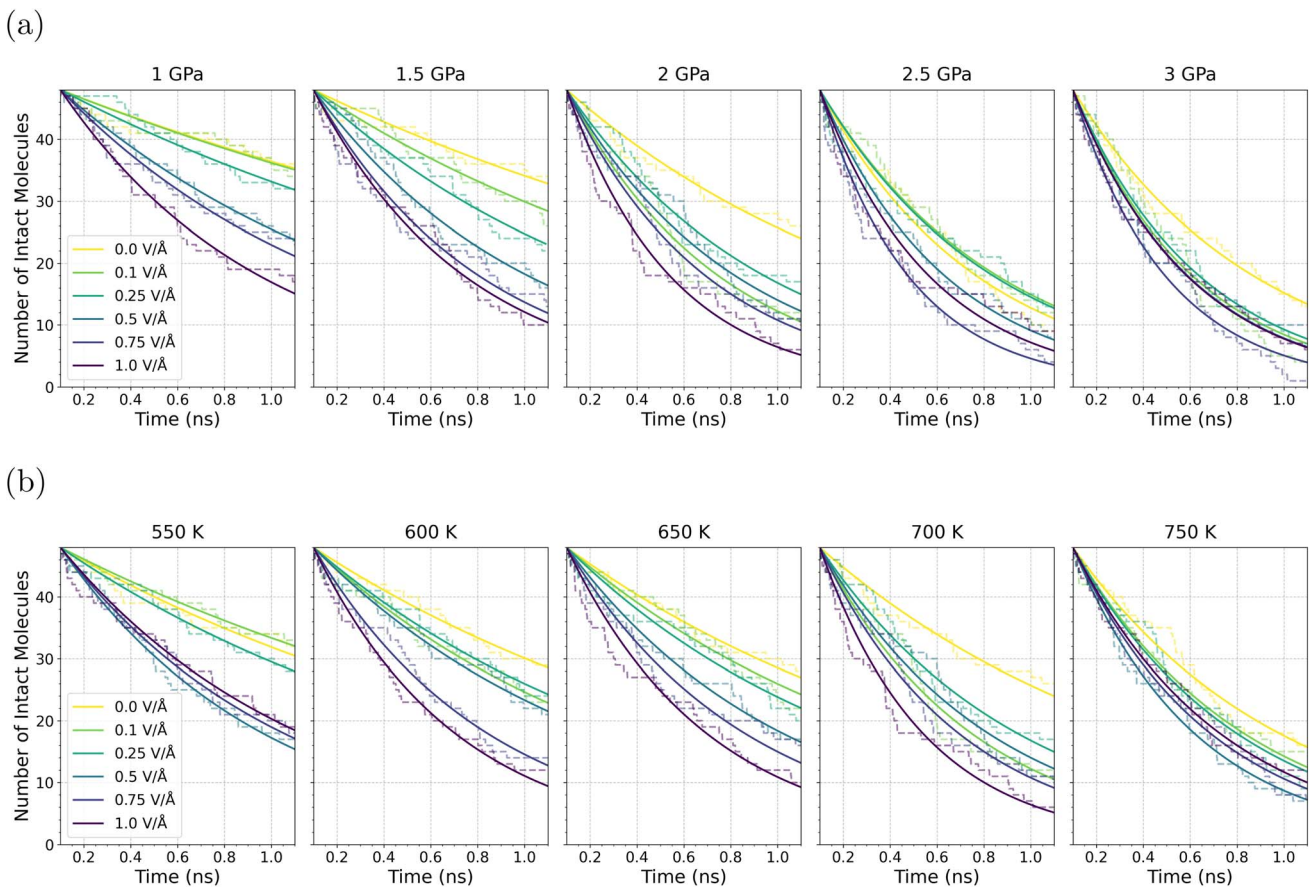

Fig. 6 Change in the number of intact TNBP molecules under different electric field strengths, at (a) 700 K under different applied pressure, and (b) 2 GPa under different temperatures. The dashed line represents the decay obtained from the MD simulations, while the solid line depicts the fitted curve of the decay using an exponential function.

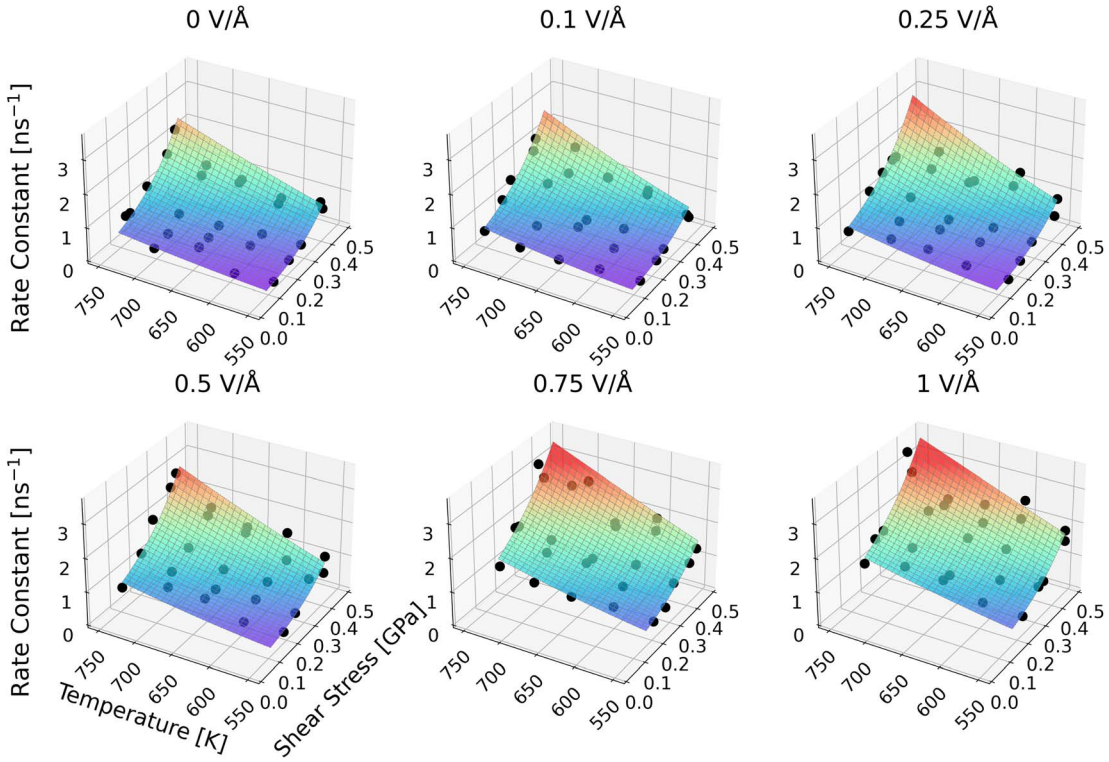

Fig. 7 Combined dependence of the rate constant for TBNP decomposition to the temperature and shear stress at different electric field strengths. 3D surface fits of the rates to the Bell model.

The Bell model parameters: E_a, ln(A), and ΔV^*, were calculated from the 3D fits, as summarized in Fig. 8 and Table S2.† The activation volume, ΔV^*, describes the dependence of rate constant on shear stress. From the 3D fits, the calculated ΔV^* was 56 ± 5 Å^3 for system without an electric field. This value is larger than our previous NEMD simulations of TNBP molecules confined between sliding pure iron surfaces,[42] which is 16 ± 3 Å^3. Therefore, the larger ΔV^* value suggests that TNBP molecules sheared between iron oxide surfaces are more mechanochemically susceptible than between iron surfaces. Both the values fall in between the values of 4 Å^3 and 130 Å^3, as calculated by Gosvami *et al.*[9] and Zhang *et al.*[10] for ZDDP tribofilm formation in experiments and other molecular mechanochemical systems.[90] The percentage of the ΔV^* compared to the molecular volume, V_{mol}, in this study is 12%, using a molecular volume V_{mol} of 440 Å^3 for the TNBP molecule.[42] This value is consistent with the 7–17% deformation ratio reported for alkyl substituent lubricants in previous studies.[76,90–92]

In the presence of an electric field, the activation volume decreased linearly as the field strength was increased. For the highest field strengths of 0.75 V Å^{-1} and 1 V Å^{-1}, ΔV^* plateaued to a value of 37 Å^3. The decrease in ΔV^* suggests a reduced dependence of mechanochemical reactions on applied stress. Considering the effect of molecular deformation in mechanochemical reactions,[93–95] this may result from competing deformation directions between shear motions and electric fields. As illustrated in Fig. 3, the electric-induced polarization leads to the separation of electronegative polar head from other atoms along z-direction. However, the shear motions was along the x-axis, the molecules were stretched and deformed more in the x-direction. Therefore, as the field increases, enhanced electric-field induced polarization became more dominant for molecular deformation compared to the shear-induced effects.

2D fits of the rate constants *versus* shear stress are shown in the ESI (Fig. S6),† and ΔV^* was computed from the slope of each line. In all cases, the activation volume ΔV^* is positive, which indicates that the rate determining step involves bond cleavage.[96] A decreasing trend in ΔV^* was also observed as the electric field increased, but with relatively large uncertainties for the 2D fits compared to the 3D fits.

The 3D fits were also used to calculate the activation energy, E_a, and the pre-exponential factor, A, as shown in Fig. 8 and Table S2.† The E_a value is significantly lower than our previous study (94 kJ mol^{-1})[43] and experiments (80 kJ mol^{-1}).[97] This underestimation of E_a is due to the high sliding velocities required by the NEMD simulations, which lead to relatively low activation energies even when the shear stress is accounted for in the Bell model.[42] E_a generally decreases with increasing electric field strength. A slight increase in E_a, from 28 kJ mol^{-1} to 30 kJ mol^{-1}, was observed from the no-field reference to when an electric field of 0.25 V Å^{-1} was applied to the system. Above 0.25 V Å^{-1} there is a linear decrease in E_a with increasing electric field strength. This observation is consistent with our previous simulations without shear[43] and has also been reported in other electric field-assisted catalysis studies.[98–101] A previous experimental study also suggested that tribofilm

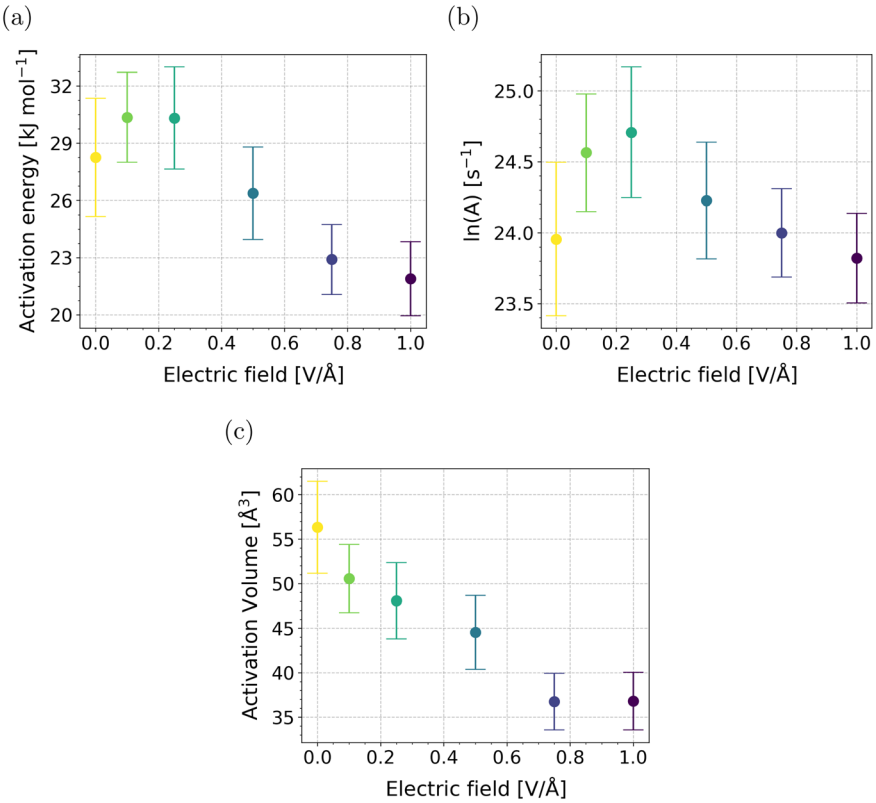

Fig. 8 Effect of the electric fields on mechanochemical parameters for TNBP molecules confined between Fe_3O_4 surfaces, change in (a) activation energy E_a, (b) natural logarithm of the pre-exponential factor ln(A), and (c) activation volume ΔV^* with external electric field strengths.

growth was accelerated by the electric field due to a reduction in E_a for the ZDDP decomposition reaction,[25] although the value of E_a was not directly quantified. The decrease in E_a is due to dipole alignment and stretching of the labile C–O bonds by the electric field.[43] A nonmonotonic variation in E_a has also been observed for mechanochemical reactions, whereby small forces slightly increase E_a and then stronger forces lead to large decreases.[102] At low electric field strengths, ln(A) also increases slightly (24 s^{-1} to 25 s^{-1}) when moving from the no-field to 0.25 V $Å^{-1}$. Under a weak electric field ($\leq$0.25 V $Å^{-1}$), the electric-field induced molecular deformation is small compared to the shear-induced deformation. The weak electric field results in a slight increase in E_a and also an enhancement in ln(A), which leads to an overall increase in reactivity compared to the no-field case. For stronger electric fields, ln(A) drops linearly with increasing field strength from 25 s^{-1} (0.25 V $Å^{-1}$) to 24 s^{-1} (1 V $Å^{-1}$). The pre-exponential factor, A, is sometimes interpreted as the collision factor, quantifying the frequency of molecule–molecule (or molecule-surface) collisions.[103] Thus, for strong fields, the number of molecule-surface collisions leading to C–O and P–O bond breaking reduces since the phosphate headgroups are all pulled towards on of the surfaces. Electric field-induced deformation dominates, leading to conformational constraints. The 2D Arrhenius fits of ln(k) *versus* 1/T are shown in the ESI (Fig. S7).† These show the same trends as the 3D fits, but with increased uncertainty.

The effective shear stress on the confined TNBP molecules increases with electric field strength (Fig. 2), which enhances the decomposition rate. The charged transition state and the products of TNBP dissociation are also electrostatically stabilized by the applied electric fields.[43,104] Meanwhile, the electric field-induced dipole alignment reduces the steric hindrance from the alkyl tails during the nucleophilic substitution reactions. Therefore, under strong electric fields, TNBP molecules decompose and polymerize more quickly. The formation of a thicker tribofilm when electric fields were applied has also been observed in experiments.[23] The rate-limiting step for mechanochemical tribofilm growth is the initial molecular decomposition.[10,76,77] This suggests that the molecular driving force for thicker tribofilm growth under strong electric fields is the reduction in the activation energy E_a for the mechanochemical decomposition. Under weak electric fields, there is a small increase in E_a, which could explain the slower tribofilm growth and increased wear seen in recent experiments with low electric potentials.[24]

Conclusions

In this study, we have used NEMD simulations with ReaxFF to investigate the mechanochemical dissociation of a trialkylphosphate, TNBP, inside the electrified contacts. The electric field-induced polarization aligns the dipoles of the polar TNBP molecules along the field direction, leading to

asymmetric atomic distributions. The phosphate anions are mainly deposited on the surface with higher electric potential (anode), while the alkyl cations are located near the lower-potential surface (cathode). The decomposed ions form covalent bonds with the surface and react through nucleophilic substitution to grow a polyphosphate tribofilm. In the presence of an electric field, longer polyphosphates are observed and they grow more quickly under electric fields compared to the no-field case. The interfacial stress also increases somewhat with electric field strength. Electrostatic stabilization of charged ions and reduced steric hindrance for nucleophilic substitution, resulting in highly polymerized phosphates. A thicker polyphosphate film generally forms under electric fields, which aligns with the thicker tribofilm observed on the anode in previous experiments.

The reaction rate constant is generally higher in the presence of an electric field and increases with the field strength. Analysing the rate constants using the Bell model shows that the dependence of mechanochemical reactions on shear stress reduces as a stronger electric field is applied, leading to smaller activation volumes. Under mild electric fields ($\leq$0.25 V Å^{-1}), electric field-induced dipole alignment competes with shear-induced axial rotation. This results in increased activation energies and pre-exponential factors. When exposed to stronger electric fields (> 0.25 V Å^{-1}), the activation energy and pre-exponential factor decrease linearly as the field strength increases. That is because the electric field-induced dipole alignment becomes more significant, resulting in more deformation-driven bond cleavage and polyphosphate formation. Our simulations help to explain conflicting experimental results, where thicker tribofilms usually form and wear is reduced under large electric potentials, while thinner films and increased wear has been observed at small electric potentials compared to the no-field case. This observation can be understood by the non-monotonic variation in the activation energy with electric field strength seen in our simulations.

Our findings provide detailed insights into the nanoscale tribofilm growth mechanism of antiwear additives at electrified interfaces, which is challenging to obtain from experiments. The methodology showcased here could help the design of lubricant additives for applications where they are exposed to external electric fields, such as electric vehicles and wind turbines. This study also paves the way for applying NEMD simulations to study the effect of external electric fields on mechanochemical synthesis in ball mills.

Data availability

All data reported in the paper can be obtained by emailing the corresponding author or tribology@imperial.ac.uk. The raw simulation data has also been deposited in a public Zenodo repository available at: **https://doi.org/10.5281/zenodo.15351368**.

Conflicts of interest

There are no conflicts to declare.

Acknowledgements

Z. Z. thanks the UK Department of Science, Innovation and Technology (DSIT), the Engineering and Physical Sciences Research Council (EPSRC), and Shell for PhD funding through an iCASE studentship (EP/X524773/1). J. P. E. was supported by DSIT and the Royal Academy of Engineering (RAEng) through the Research Fellowships scheme. We acknowledge the use of Imperial College London Research Computing Service (**https://doi.org/10.14469/hpc/2232**) and the UK Materials and Molecular Modelling Hub, which is partially funded by the EPSRC (EP/T022213/1, EP/W032260/1 and EP/P020194/1). We thank Efstratios M. Kritikos (Caltech), Andrea Giusti and Daniele Dini (Imperial College London) for useful discussions.

References

1 R. T. O. Neill and R. Boulatov, The many flavours of mechanochemistry and its plausible conceptual underpinnings, *Nat. Rev. Chem.*, 2021, **5**, 148–167.
2 V. Martinez, T. Stolar, B. Karadeniz, I. Brekalo and K. Užarević, Advancing mechanochemical synthesis by combining milling with different energy sources, *Nat. Rev. Chem.*, 2023, **7**, 51–65.
3 Y. Li, N. L. Haworth, L. Xiang, S. Ciampi, M. L. Coote and N. Tao, Mechanical Stretching-Induced Electron-Transfer Reactions and Conductance Switching in Single Molecules, *J. Am. Chem. Soc.*, 2017, **139**, 14699–14706.
4 T. Scheele and T. Neudecker, Using oriented external electric fields to manipulate rupture forces of mechanophores, *Phys. Chem. Chem. Phys.*, 2023, **25**, 28070–28077.
5 Y. S. Zholdassov, R. W. Kwok, M. A. Shlain, M. Patel, M. Marianski and A. B. Braunschweig, Kinetics of primary mechanochemical covalent-bond-forming reactions, *RSC Mechanochem.*, 2024, **1**, 11–32.
6 M. M. Mokhtar, T. Heppler and J. Mack, Mechanochemically mediated electrosynthesis: unveiling a new pathway for redox reactions under mechanochemical conditions, *Green Chem.*, 2025, DOI: **10.1039/D4GC06293K**.
7 Z. Wang, X. Dong, W. Tang and Z. L. Wang, Contact-electrocatalysis (CEC), *Chem. Soc. Rev.*, 2024, **53**, 4349–4373.
8 A. Boscoboinik, D. Olson, H. Adams, N. Hopper and W. T. Tysoe, Measuring and modelling mechanochemical reaction kinetics, *Chem. Commun.*, 2020, **56**, 7730–7733.
9 N. N. Gosvami, J. A. Bares, F. Mangolini, A. R. Konicek, D. G. Yablon and R. W. Carpick, Mechanisms of antiwear tribofilm growth revealed in situ by single-asperity sliding contacts, *Science*, 2015, **348**, 102–106.
10 J. Zhang, J. P. Ewen, M. Ueda, J. S. Wong and H. A. Spikes, Mechanochemistry of Zinc Dialkyldithiophosphate on Steel Surfaces under Elastohydrodynamic Lubrication Conditions, *ACS Appl. Mater. Interfaces*, 2020, **12**, 6662–6676.
11 H. Spikes, Mechanisms of ZDDP—An Update, *Tribol. Lett.*, 2025, **73**, 38.

12 Y. Chen, S. Jha, A. Raut, W. Zhang and H. Liang, Performance Characteristics of Lubricants in Electric and Hybrid Vehicles: A Review of Current and Future Needs, *Front. Mech. Eng.*, 2020, **6**, 571464.
13 W. Holweger, L. Bobbio, Z. Mo, J. Fliege, B. Goerlach and B. Simon, A Validated Computational Study of Lubricants under White Etching Crack Conditions Exposed to Electrical Fields, *Lubricants*, 2023, **11**, 45.
14 K. Nakayama and J. M. Martin, Tribochemical reactions at and in the vicinity of a sliding contact, *Wear*, 2006, **261**, 235–240.
15 H. A. Spikes, Triboelectrochemistry: Influence of Applied Electrical Potentials on Friction and Wear of Lubricated Contacts, *Tribol. Lett.*, 2020, **68**, 1–27.
16 R. S. Notay, A Brief Review on the Tribological Effects of Electrically Induced Bearing Damage, *J. Tribol.*, 2025, **147**, 051112.
17 S. S. Wang, S. P. Maheswari and S. C. Tung, The nature of electrochemical reactions between several zinc organodithiophosphate antiwear additives and cast iron surfaces, *Tribol. Trans.*, 1989, **32**, 91–98.
18 Y. Yamamoto and F. Hirano, Scuffing resistance of phosphate esters II: Effect of applied voltage, *Wear*, 1981, **66**, 77–86.
19 S. C. Tung and S. S. Wang, Friction reduction from electrochemically deposited films, *Tribol. Trans.*, 1991, **34**, 23–34.
20 S. C. Tung and S. S. Wang, In-situ electro-charging for friction reduction and wear resistant film formation, *Tribol. Trans.*, 1991, **34**, 479–488.
21 X. Xu and H. Spikes, Study of zinc dialkyldithiophosphate in di-ethylhexyl sebacate using electrochemical techniques, *Tribol. Lett.*, 2007, **25**, 141–148.
22 G. W. Stachowiak and A. W. Batchelor, Fretting and Minor Wear Mechanisms, *Eng. Tribol.*, 2006, 621–650.
23 G. X. Xie, G. Li, J. B. Luo and S. H. Liu, Effects of electric field on characteristics of nano-confined lubricant films with ZDDP additive, *Tribol. Int.*, 2010, **43**, 975–980.
24 A. Yousuf, H. Spikes, L. Guo and A. Kadiric, Influence of Electric Potentials on Surface Damage in Rolling–Sliding Contacts Under Mixed Lubrication, *Tribol. Lett.*, 2025, **73**, 45.
25 H. Cao and Y. Meng, Electrochemical effect on boundary lubrication of ZDDP additive blended in propylene carbonate/diethyl succinate, *Tribol. Int.*, 2018, **126**, 229–239.
26 M. K. A. Ali, Y. Sun, C. Zhang, Q. Yu, C. Zhao, F. Zhou and W. Liu, Improving Tribological Performance of Electrified Steel Interfaces in E-Mobility Systems Using Ash-Sulfur-Less Oil Additives Based on Amine Salts-Phosphoric Esters, *Tribol. Int.*, 2025, **205**, 110561.
27 J. P. Ewen, D. M. Heyes and D. Dini, Advances in nonequilibrium molecular dynamics simulations of lubricants and additives, *Friction*, 2018, **6**, 349–386.
28 A. Martini, S. J. Eder and N. Dörr, Tribochemistry: A Review of Reactive Molecular Dynamics Simulations, *Lubricants*, 2020, **8**, 44.
29 N. J. English and C. J. Waldron, Perspectives on external electric fields in molecular simulation: progress, prospects and challenges, *Phys. Chem. Chem. Phys.*, 2015, **17**, 12407–12440.
30 O. Y. Fajardo, F. Bresme, A. A. Kornyshev and M. Urbakh, Electrotunable Friction with Ionic Liquid Lubricants: How Important Is the Molecular Structure of the Ions?, *J. Phys. Chem. Lett.*, 2015, **6**, 3998–4004.
31 K. Pivnic, F. Bresme, A. A. Kornyshev and M. Urbakh, Electrotunable Friction in Diluted Room Temperature Ionic Liquids: Implications for Nanotribology, *ACS Appl. Nano Mater.*, 2020, **3**, 10708–10719.
32 S. Di Lecce, A. A. Kornyshev, M. Urbakh and F. Bresme, Electrotunable Lubrication with Ionic Liquids: The Effects of Cation Chain Length and Substrate Polarity, *ACS Appl. Mater. Interfaces*, 2020, **12**, 4105–4113.
33 F. Bresme, A. A. Kornyshev, S. Perkin and M. Urbakh, Electrotunable friction with ionic liquid lubricants, *Nat. Mater.*, 2022, **21**, 848–858.
34 X. Ruan, X. Wang, Y. Zhao, R. Zhou, L. Bao, F. Zhou and Z. Lu, Tribochemical Mechanism of Ionic Liquid [P6,6,6,14][BEHP] on Ferrous Surfaces, *Tribol. Int.*, 2025, **208**, 110643.
35 Y. Chen, M. Ji, F. Zhang, J. Li, H. Pan, Y. Zhao, Z. Zhang and L. Liu, Investigation of Tribological Behavior and Lubrication Mechanisms of Zinc Oxide under Poly α-olefin Lubrication Enhanced by the Electric Field, *Langmuir*, 2024, **40**, 6741–6749.
36 M. M. Gianetti, R. Guerra, A. Vanossi, M. Urbakh and N. Manini, Electric-field frictional effects in confined zwitterionic molecules, *Phys. Chem. Chem. Phys.*, 2023, **25**, 19037–19045.
37 T. P. Senftle, S. Hong, M. M. Islam, S. B. Kylasa, Y. Zheng, Y. K. Shin, C. Junkermeier, R. Engel-Herbert, M. J. Janik, H. M. Aktulga, *et al.*, The ReaxFF reactive force-field: development, applications and future directions, *npj Comput. Mater.*, 2016, **2**, 15011.
38 M. T. Devlin, J. Guevremont, R. Sheets, J. Loper, G. Guinther, K. Thompson and T.-C. Jao, Effect of metal-free phosphorus anti-wear compounds on passenger car emissions and fuel economy, *Lubric. Sci.*, 2008, **20**, 151–161.
39 M. Lorenz, A. A. Pawlicki, H. E. Hysmith, K. Cogen, H. Thaker and O. S. Ovchinnikova, Direct Multimodal Nanoscale Visualization of Early Phosphorus-Based Antiwear Tribofilm Formation, *ACS Appl. Mater. Interfaces*, 2022, **14**, 35157–35166.
40 D. Sung and A. J. Gellman, The surface chemistry of alkyl and arylphosphate vapor phase lubricants on Fe foil, *Tribol. Int.*, 2002, **35**, 579–590.
41 J. P. Ewen, C. A. Latorre, C. Gattinoni, A. Khajeh, J. D. Moore, J. E. Remias, A. Martini and D. Dini, Substituent Effects on the Thermal Decomposition of Phosphate Esters on Ferrous Surfaces, *J. Phys. Chem. C*, 2020, **124**, 9852–9865.
42 C. Ayestarán Latorre, J. E. Remias, J. D. Moore, H. A. Spikes, D. Dini and J. P. Ewen, Mechanochemistry of phosphate

esters confined between sliding iron surfaces, *Commun. Chem.*, 2021, **4**, 178.
43 Z. Zhu, J. P. Ewen, E. M. Kritikos, A. Giusti and D. Dini, Effect of Electric Fields on the Decomposition of Phosphate Esters, *J. Phys. Chem. C*, 2024, **128**, 15959–15973.
44 R. D. Evans, K. L. More, C. V. Darragh and H. P. Nixon, Transmission Electron Microscopy of Boundary-Lubricated Bearing Surfaces. Part II: Mineral Oil Lubricant with Sulfur-and Phosphorus-Containing Gear Oil Additives, *Tribol. Trans.*, 2005, **48**, 299–307.
45 D. R. Wheeler and O. D. Faut, The adsorption and thermal decomposition of tricresylphosphate (TCP) on iron and gold, *Appl. Surf. Sci.*, 1984, **18**, 106–122.
46 F. T. Barcroft and S. G. Daniel, The action of neutral organic phosphates as EP additives, *J. Basic Eng.*, 1965, **87**, 761–767.
47 A. P. Thompson, H. M. Aktulga, R. Berger, D. S. Bolintineanu, W. M. Brown, P. S. Crozier, P. J. in't Veld, A. Kohlmeyer, S. G. Moore, T. D. Nguyen, *et al.*, LAMMPS - a flexible simulation tool for particle-based materials modeling at the atomic, meso, and continuum scales, *Comput. Phys. Commun.*, 2022, **271**, 108171.
48 L. Verlet, Computer "Experiments" on Classical Fluids. I. Thermodynamical Properties of Lennard-Jones Molecules, *Phys. Rev.*, 1967, **159**, 98.
49 A. C. Van Duin, S. Dasgupta, F. Lorant and W. A. Goddard, ReaxFF: a reactive force field for hydrocarbons, *J. Phys. Chem. A*, 2001, **105**, 9396–9409.
50 K. Chenoweth, A. C. T. Van Duin and W. A. Goddard, ReaxFF Reactive Force Field for Molecular Dynamics Simulations of Hydrocarbon Oxidation, *J. Phys. Chem. A*, 2008, **112**, 1040–1053.
51 H. M. Aktulga, J. C. Fogarty, S. A. Pandit and A. Y. Grama, Parallel reactive molecular dynamics: Numerical methods and algorithmic techniques, *Parallel Comput.*, 2012, **38**, 245–259.
52 A. Khajeh, X. Hu, K. Mohammadtabar, Y. K. Shin, A. C. Van Duin, S. Berkebile and A. Martini, Statistical Analysis of Tri-Cresyl Phosphate Conversion on an Iron Oxide Surface Using Reactive Molecular Dynamics Simulations, *J. Phys. Chem. C*, 2019, **123**, 12886–12893.
53 A. Khajeh, F. H. Bhuiyan, J.-E. Mogonye and A. Martini, Thermal Decomposition of Tricresyl Phosphate on Ferrous Surfaces, *J. Phys. Chem. C*, 2021, **125**, 5076–5087.
54 E. Ogbomo, F. H. Bhuiyan, C. A. Latorre, A. Martini and J. P. Ewen, Effects of surface chemistry on the mechanochemical decomposition of tricresyl phosphate, *Phys. Chem. Chem. Phys.*, 2023, **26**, 278–292.
55 Q. Yang and F. Duan, Tribological Properties of Phosphate Ester Confined between Iron-Based Surfaces, *Langmuir*, 2024, **40**, 3738–3747.
56 Q. Tian and H. Liu, Densities and viscosities of binary mixtures of tributyl phosphate with hexane and dodecane from (298.15 to 328.15) K, *J. Chem. Eng. Data*, 2007, **52**, 892–897.
57 T. Schneider and E. Stoll, Molecular-dynamics study of a three-dimensional one-component model for distortive phase transitions, *Phys. Rev. B: Condens. Matter Mater. Phys.*, 1978, **17**, 1302.
58 A. Stukowski, Visualization and analysis of atomistic simulation data with OVITO–the Open Visualization Tool, *Model. Simulat. Mater. Sci. Eng.*, 2009, **18**, 015012.
59 J. Chen and T. J. Martínez, QTPIE: Charge transfer with polarization current equalization. A fluctuating charge model with correct asymptotics, *Chem. Phys. Lett.*, 2007, **438**, 315–320.
60 A. K. Rappé and W. A. Goddard, Charge equilibration for molecular dynamics simulations, *J. Phys. Chem.*, 1991, **95**, 3358–3363.
61 E. Kritikos and A. Giusti, Reactive molecular dynamics investigation of toluene oxidation under electrostatic fields: Effect of the modeling of local charge distribution, *J. Phys. Chem. A*, 2020, **124**, 10705–10716.
62 J. Chen, D. Hundertmark and T. J. Martínez, A unified theoretical framework for fluctuating-charge models in atom-space and in bond-space, *J. Chem. Phys.*, 2008, **129**, 214113.
63 T. Gergs, S. Dirkmann and T. Mussenbrock, Integration of external electric fields in molecular dynamics simulation models for resistive switching devices, *J. Appl. Phys.*, 2018, **123**, 245301.
64 E. M. Kritikos, A. Lele, A. C. Van Duin and A. Giusti, Atomistic insight into the effects of electrostatic fields on hydrocarbon reaction kinetics, *J. Chem. Phys.*, 2023, **158**, 54109.
65 J. Chen and T. J. Martínez, Charge conservation in electronegativity equalization and its implications for the electrostatic properties of fluctuating-charge models, *J. Chem. Phys.*, 2009, **131**, 44114.
66 J. Chen and T. J. Martínez, The Dissociation Catastrophe in Fluctuating-Charge Models and its Implications for the Concept of Atomic Electronegativity, *Prog. Theor. Chem. Phys.*, 2009, **19**, 397–415.
67 L. I. Farfan-Cabrera, A. Erdemir, J. A. Cao-Romero-Gallegos, I. Alam and S. Lee, Electrification effects on dry and lubricated sliding wear of bearing steel interfaces, *Wear*, 2023, **516–517**, 204592.
68 O. A. Aguilar-Rosas, L. I. Farfan-Cabrera, A. Erdemir and J. A. Cao-Romero-Gallegos, Electrified four-ball testing - a potential alternative for assessing lubricants (E-fluids) for electric vehicles, *Wear*, 2023, 204676.
69 H. Lang, K. Zou, R. Chen, Y. Huang and Y. Peng, Role of Interfacial Water in the Tribological Behavior of Graphene in an Electric Field, *Nano Lett.*, 2022, **22**, 6055–6061.
70 L. Guo, H. Mol, T. Nijdam, L. de Vries and J. Bongaerts, Study on the Electric Discharge Behaviour of a Single Contact in EV Motor Bearings, *Tribol. Int.*, 2023, 108743.
71 J. F. Archard and M. T. Kirk, Lubrication at point contacts, *Proc. R. Soc. London, Ser. A*, 1961, **261**, 532–550.
72 S. Raghuraman, M. Soleymaniha, Z. Ye and J. R. Felts, The role of mechanical force on the kinetics and dynamics of electrochemical redox reactions on graphene, *Nanoscale*, 2018, **10**, 17912–17923.

73 M. A. Wood, A. C. Van Duin and A. Strachan, Coupled thermal and electromagnetic induced decomposition in the molecular explosive αhMX; A reactive molecular dynamics study, *J. Phys. Chem. A*, 2014, **118**, 885–895.
74 J. Zhang and W. Guo, The role of electric field on decomposition of CL-20/HMX cocrystal: A reactive molecular dynamics study, *J. Comput. Chem.*, 2021, **42**, 2202–2212.
75 J. Zhang and H. Spikes, On the Mechanism of ZDDP Antiwear Film Formation, *Tribol. Lett.*, 2016, **63**, 1–15.
76 J. Zhang, J. P. Ewen and H. A. Spikes, Substituent effects on the mechanochemical response of zinc dialkyldithiophosphate, *Mol. Syst. Des. Eng.*, 2022, **7**, 1045–1055.
77 L. Fang, S. Korres, W. A. Lamberti, M. N. Webster and R. W. Carpick, What stress components drive mechanochemistry? A study of ZDDP tribofilm formation, *Faraday Discuss.*, 2023, **241**, 394–412.
78 H. Spikes, Stress-augmented thermal activation: Tribology feels the force, *Friction*, 2018, **6**, 1–31.
79 G. I. Bell, Models for the Specific Adhesion of Cells to Cells, *Science*, 1978, **200**, 618–627.
80 A. C. Aragonès, N. L. Haworth, N. Darwish, S. Ciampi, N. J. Bloomfield, G. G. Wallace, I. Diez-Perez and M. L. Coote, Electrostatic catalysis of a Diels-Alder reaction, *Nature*, 2016, **531**, 88–91.
81 W. Quapp, J. M. Bofill and J. Ribas-Ariño, Analysis of the Acting Forces in a Theory of Catalysis and Mechanochemistry, *J. Phys. Chem. A*, 2017, **121**, 2820–2838.
82 C. Liu, Y. Tian and Y. A. Meng, Chemical Potential Equation for Modeling Triboelectrochemical Reactions on Solid–Liquid Interfaces, *Front. Chem.*, 2021, **9**, 650880.
83 J. Gao, W. D. Luedtke, D. Gourdon, M. Ruths, J. N. Israelachvili and U. Landman, Frictional Forces and Amontons' Law: From the Molecular to the Macroscopic Scale, *J. Phys. Chem. B*, 2004, **108**, 3410–3425.
84 S. J. Eder, A. Vernes and G. Betz, On the Derjaguin Offset in Boundary-Lubricated Nanotribological Systems, *Langmuir*, 2013, **29**, 13760–13772.
85 G. Cassone and F. Martelli, Electrofreezing of liquid water at ambient conditions, *Nat. Commun.*, 2024, **15**, 1856.
86 R. Heuberger, A. Rossi and N. D. Spencer, XPS study of the influence of temperature on ZnDTP tribofilm composition, *Tribol. Lett.*, 2007, **25**, 185–196.
87 H. Spikes, The history and mechanisms of ZDDP, *Tribol. Lett.*, 2004, **17**, 469–489.
88 S. Ntioudis, J. P. Ewen, D. Dini and C. H. Turner, A hybrid off-lattice kinetic Monte Carlo/molecular dynamics method for amorphous thin film growth, *Comput. Mater. Sci.*, 2023, **229**, 112421.
89 M. Ueda and H. Spikes, ZDDP Tribofilm Formation and Removal, *Tribol. Lett.*, 2024, **72**, 109.
90 A. Martini and S. H. Kim, Activation Volume in Shear-Driven Chemical Reactions, *Tribol. Lett.*, 2021, **69**, 1–14.
91 X. He and S. H. Kim, Mechanochemistry of Physisorbed Molecules at Tribological Interfaces: Molecular Structure Dependence of Tribochemical Polymerization, *Langmuir*, 2017, **33**, 2717–2724.
92 J. Yeon, X. He, A. Martini and S. H. Kim, Mechanochemistry at Solid Surfaces: Polymerization of Adsorbed Molecules by Mechanical Shear at Tribological Interfaces, *ACS Appl. Mater. Interfaces*, 2017, **9**, 3142–3148.
93 A. Khajeh, X. He, J. Yeon, S. H. Kim and A. Martini, Mechanochemical Association Reaction of Interfacial Molecules Driven by Shear, *Langmuir*, 2018, **34**, 5971–5977.
94 X. He and S. H. Kim, Surface Chemistry Dependence of Mechanochemical Reaction of Adsorbed Molecules - An Experimental Study on Tribopolymerization of α-Pinene on Metal, Metal Oxide, and Carbon Surfaces, *Langmuir*, 2018, **34**, 2432–2440.
95 F. H. Bhuiyan, Y. S. Li, S. H. Kim and A. Martini, Shear-activation of mechanochemical reactions through molecular deformation, *Sci. Rep.*, 2024, **14**(1), 1–12.
96 B. Chen, R. Hoffmann and R. Cammi, The Effect of Pressure on Organic Reactions in Fluids—a New Theoretical Perspective, *Angew. Chem., Int. Ed.*, 2017, **56**, 11126–11142.
97 L. Cho and E. E. Klaus, Oxidative Degradation of Phosphate Esters, *ASLE Trans.*, 1981, **24**, 119–124.
98 F. Che, J. T. Gray, S. Ha and J.-S. McEwen, Improving Ni Catalysts Using Electric Fields: A DFT and Experimental Study of the Methane Steam Reforming Reaction, *ACS Catal.*, 2017, **7**, 551–562.
99 G. Cassone, F. Pietrucci, F. Saija, F. Guyot and A. M. Saitta, One-step electric-field driven methane and formaldehyde synthesis from liquid methanol, *Chem. Sci.*, 2017, **8**, 2329–2336.
100 G. Cassone, A. Sofia, G. Rinaldi and J. Sponer, Catalyst-Free Hydrogen Synthesis from Liquid Ethanol: An ab Initio Molecular Dynamics Study, *J. Phys. Chem. C*, 2019, **123**, 9202–9208.
101 S. Zhao, K. Gong, Z. Song, G. Cassone and J. Xie, Exploring the Linear Energy Relationships between Activation Energy and Reaction Energy under an Electric Field, *J. Chem. Theory Comput.*, 2025, **21**, 4625.
102 M. Krupicka and D. Marx, Disfavoring Mechanochemical Reactions by Stress-Induced Steric Hindrance, *J. Chem. Theory Comput.*, 2015, **11**, 841–846.
103 M. G. Evans and M. Polanyi, Some applications of the transition state method to the calculation of reaction velocities, especially in solution, *Trans. Faraday Soc.*, 1935, **31**, 875–894.
104 N. G. Léonard, R. Dhaoui, T. Chantarojsiri and J. Y. Yang, Electric Fields in Catalysis: From Enzymes to Molecular Catalysts, *ACS Catal.*, 2021, **11**, 10923–10932.